

Cite this: *J. Mater. Chem. A*, 2017, 5, 8493

A highly stable non-noble metal Ni₂P co-catalyst for increased H₂ generation by g-C₃N₄ under visible light irradiation†

Ping Ye,^a Xinling Liu,^a James Icozzia,^b Yupeng Yuan,^{*ab} Lina Gu,^a Gengsheng Xu^a and Zhiquan Lin^{id}^{*b}

Nickel phosphide (Ni₂P) was grown on a graphitic carbon nitride (g-C₃N₄) surface by annealing a mixture of g-C₃N₄, NiCl₂, and NaH₂PO₂ at 400 °C for 2 h in an Ar atmosphere. During the annealing, Ni₂P particles formed intimate interfaces with g-C₃N₄. As a result, charge transfer from photo-excited g-C₃N₄ to Ni₂P was improved as demonstrated by the improved photocatalytic H₂ generation (40.5 μmol h⁻¹ g⁻¹) compared to a physical mixture of Ni₂P and g-C₃N₄ (trace H₂ generation). Under optimal and identical experimental conditions, the H₂ production rate on Ni₂P-loaded g-C₃N₄ (2 wt%) is 82.5 μmol h⁻¹ g⁻¹, which is higher than that of Pt-loaded g-C₃N₄ (0.5 wt%) (72 μmol h⁻¹ g⁻¹). Impressively, Ni₂P shows a highly stable H₂ production activity despite being a non-noble metal co-catalyst. No activity loss occurs over repeated use and 24 h long-term H₂ generation trials. In contrast, a pronounced reduction in H₂ generation was observed for Pt-loaded g-C₃N₄ (0.5 wt%) over the same 24 hour trial period. Among their many advantages, including non-toxicity, low cost and natural abundance, Ni₂P/g-C₃N₄ composites are a promising alternative for realizing efficient, long-lasting photocatalytic H₂ production.

Received 1st February 2017
Accepted 3rd April 2017

DOI: 10.1039/c7ta01031a

rsc.li/materials-a

Introduction

Molecular hydrogen (H₂) is regarded as a renewable and environmentally friendly chemical fuel to replace fossil fuels due to its high energy density and water-only by-product. Of the available techniques, H₂ production from water splitting by solar irradiation of a photocatalyst is an ideal route. In recent years, hundreds of semiconductors have been investigated for photocatalytic H₂ production *via* exposure to ultraviolet and/or visible light irradiation.^{1–9} Researchers recognize that suitable co-catalyst coupling with photocatalysts is essential for realizing active photocatalytic H₂ production. A desirable co-catalyst has two functions: serves as an electron sink to draw electrons from the photo-excited semiconductor and a catalyst to lower the H₂ generation overpotential.^{10,11} Despite their exceptional activity, the natural scarcity of noble metals limits their utility as co-catalysts. For economically viable H₂ generation, co-catalysts made from earth-abundant materials are needed. Several non-noble metal-based materials, such as MoS₂, NiS_x, and Ni(OH)₂ have been shown to be efficient co-catalysts for active H₂ generation when deposited onto the surface of photo-

catalysts.^{12–15} Recently, transition metal phosphides (MPs), including Ni₂P, FeP, CoP, MoP, and Cu₃P have been investigated as H₂ evolution co-catalysts.^{16–22} Though the H₂ generation mechanism for these metal phosphide co-catalysts is not yet fully understood, coupling these co-catalysts with various photocatalysts to achieve efficient H₂ generation remains a worthwhile venture as mechanistic questions are worked out in parallel.

In recent years, g-C₃N₄ has received much attention due to its stability and efficiency in photocatalytic H₂ evolution under visible light exposure.^{23,24} Noble metal Pt is a typical co-catalyst employed to promote H₂ generation on g-C₃N₄. However, Pt is not only costly but also suffers from the back reaction with H₂ and O₂ to produce H₂O during longer H₂ production trials.²⁵ Most recently, Xu *et al.* has prepared g-C₃N₄ materials through a urea polymerization method and subsequently loaded Ni₂P onto the g-C₃N₄ catalyst *via* a two-step procedure. Ni(OH)₂ was grown *in situ* on g-C₃N₄ by using a hydrothermal method and then phosphidated into Ni₂P to obtain the final Ni₂P/g-C₃N₄ hybrid.²⁶ This work validates the role of Ni₂P in boosting H₂ generation and serving as a replacement for expensive Pt. It is well known that photocatalytic H₂ generation is dependent on the synthesis strategy of the co-catalyst and photocatalyst. In addition, the choice of precursors controls the physiochemical properties of g-C₃N₄. It is for these reasons that it is essential to investigate the many potential synthesis and processing strategies available for producing, ostensibly, the same final product. As is well known, g-C₃N₄ derived from melamine offers

^aSchool of Chemistry and Chemical Engineering, Anhui University, Hefei 230036, P. R. China. E-mail: yupengyuan@ahu.edu.cn

^bSchool of Materials Science and Engineering, Georgia Institute of Technology, Atlanta, GA 30332, USA. E-mail: zhiquan.lin@mse.gatech.edu

† Electronic supplementary information (ESI) available. See DOI: 10.1039/c7ta01031a

exceptional stability for H₂ generation, making melamine to be the most suitable precursor for verifying the stability of the non-noble metal co-catalyst. From a technological view point, the formation of Ni₂P and g-C₃N₄ composites *via* a facile one-step procedure is highly desirable. Herein, we loaded Ni₂P onto g-C₃N₄ through facile annealing of a mixture of NiCl₂, NaH₂PO₂ and g-C₃N₄ in an Ar atmosphere wherein the g-C₃N₄ was prepared by melamine condensation. We find that g-C₃N₄/Ni₂P composites can be facilely formed in a one-step procedure, which avoids the tedious manipulation of hydrothermal synthesis in Xu's work. The as-obtained g-C₃N₄/Ni₂P composites offer highly stable H₂ generation. To the best of our knowledge, this work is the first report on a facile one step preparation technique for g-C₃N₄ and Ni₂P hybrids with highly stable H₂ generation. Moreover, the present work clearly shows the potential of metal phosphides to serve as co-catalysts for improved H₂ generation.

Experimental

Synthesis of Ni₂P/g-C₃N₄ hybrids

All reagents were used as received. g-C₃N₄ was prepared by direct polycondensation of melamine in air at 520 °C for 2 hours at a heating rate of 2.3 °C min⁻¹. The Ni₂P co-catalyst was grown on g-C₃N₄ through a single-step thermal annealing process. Samples with different loading amounts of Ni₂P (1 wt%, 2 wt%, 4 wt%, and 8 wt%) were labelled g-C₃N₄/Ni₂P (1 wt%), g-C₃N₄/Ni₂P (2 wt%), g-C₃N₄/Ni₂P (4 wt%), and g-C₃N₄/Ni₂P (8 wt%), respectively. In a typical preparation of 2 wt% Ni₂P-loaded g-C₃N₄, g-C₃N₄ (800 mg), NiCl₂·6H₂O (50 mg), and NaH₂PO₂·H₂O (84 mg) were mixed *via* a mortar and pestle. The mixture was then heated at 400 °C for 2 hours in an Ar atmosphere at a heating rate of 2 °C min⁻¹ in a tube furnace. After cooling down to room temperature, the product was washed with deionized water and ethanol three times and finally dried at 60 °C overnight. Pure Ni₂P particles were also prepared using a similar procedure in the absence of g-C₃N₄.²⁷

Characterization

Powder X-ray diffraction (XRD) data were collected on a DX-2700 X-ray diffractometer using CuK_{α1} radiation. The acceleration voltage and applied current were 40 kV and 30 mA, respectively. Morphology was observed by scanning electron microscopy (SEM, Hitachi S-4800) and transmission electron microscopy (TEM, JEOL JEM-2100F). UV-vis diffuse reflectance spectra (DRS) were measured on a HITACHI U-3900 UV-Vis spectrophotometer. The photoluminescence (PL) spectra were recorded on a HITACHI F-4600 fluorometer at an excitation wavelength of 320 nm. Time-resolved PL spectra measurements were performed on a HORIB Fluoro Max-4P spectrometer with an excitation wavelength of 320 nm.

Photocatalytic measurements

Photocatalytic H₂ generation was measured in an 80 mL closed Pyrex reactor with a quartz window under visible light irradiation. The photo-catalyst (20 mg) was dispersed in 20 mL of

triethanolamine (TEOA) aqueous solution. The reactor was then bubbled with Ar for 30 min to remove air. Photocatalytic H₂ evolution was then initiated by irradiating the suspension using a 300 W xenon lamp. A cut-off filter ($\lambda \geq 420$ nm) was equipped to provide only visible light. The gaseous product was analyzed by gas chromatography (GC-1690, Kexiao, China) with a TCD detector. The photocatalytic H₂ generation on Pt/g-C₃N₄ and a physical mixture of Ni₂P and g-C₃N₄ was also tested for comparison. Pt (0.5 wt%) was *in situ* deposited on g-C₃N₄ by injecting small amounts of H₂PtCl₆ solution (212 μ L, 1 g L⁻¹) into the reactor. Ni₂P (2 mg) and g-C₃N₄ (98 mg) powders were dispersed in TEOA solution for testing the H₂ generation from the physically mixed Ni₂P and g-C₃N₄ system.

Results and discussion

Sample characterization

The XRD patterns of g-C₃N₄/Ni₂P are illustrated in Fig. 1. g-C₃N₄/Ni₂P (2 wt%), g-C₃N₄/Ni₂P (4 wt%), and g-C₃N₄/Ni₂P (8 wt%) preparations were used as representative samples for this work. All peaks can be indexed to g-C₃N₄ and Ni₂P with no evidence of side product formation occurring during the thermal annealing process for Ni₂P. The characteristic peaks at 13° and 27.4° are evidence of the periodic in-plane tri-s-triazine motif stacking and interlayer aromatic packing. The peaks at 40.77°, 44.59°, 47.45°, and 54.16° correspond to Ni₂P. These peaks become more intense at higher Ni₂P loading contents. The FT-IR analysis (Fig. S1†) further supports the fact that the original g-C₃N₄ backbones are retained after Ni₂P hybridization. Although no new vibrational peaks belonging to P- and Ni-

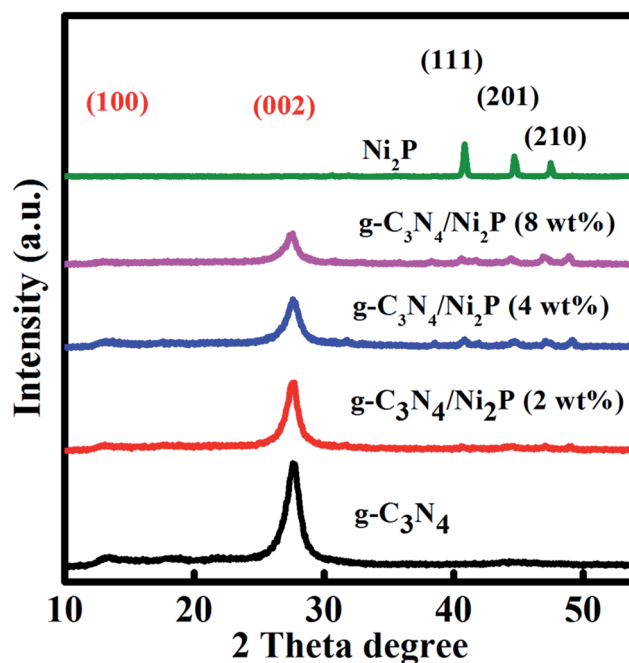


Fig. 1 XRD patterns of pure g-C₃N₄, pure Ni₂P and g-C₃N₄/Ni₂P composites with different Ni₂P contents (2 wt%, 4 wt%, and 8 wt%). The facet indices in red correspond to g-C₃N₄ and the indices in black correspond to Ni₂P.

related groups in $g\text{-C}_3\text{N}_4/\text{Ni}_2\text{P}$ hybrids were detected in FT-IR spectra, the shift of the Ni 2p (Fig. S2†), P 2p (Fig. S3†), C 1s (Fig. S4†) and N 1s (Fig. S5†) binding energies in $g\text{-C}_3\text{N}_4/\text{Ni}_2\text{P}$ (8 wt%) hybrids compared to pure Ni_2P and $g\text{-C}_3\text{N}_4$ or physical mixtures of Ni_2P and $g\text{-C}_3\text{N}_4$ demonstrates that the annealing process for Ni_2P hybridization likely initiates new chemical bonding between Ni_2P and $g\text{-C}_3\text{N}_4$.

The UV-vis spectra (Fig. 2) of $g\text{-C}_3\text{N}_4/\text{Ni}_2\text{P}$ hybrids show the typical absorption edge of $g\text{-C}_3\text{N}_4$ at 460 nm. The absorption edge of $g\text{-C}_3\text{N}_4/\text{Ni}_2\text{P}$ hybrids becomes more intense in the visible light region with increasing Ni_2P loading onto $g\text{-C}_3\text{N}_4$. This supports the increased Ni_2P content in $g\text{-C}_3\text{N}_4/\text{Ni}_2\text{P}$ samples. This phenomenon is further verified by the Ni_2P absorption spectrum. In comparison, the physical mixture of $g\text{-C}_3\text{N}_4$ and Ni_2P (2 wt%) offers inferior light absorption behaviour when compared to $g\text{-C}_3\text{N}_4/\text{Ni}_2\text{P}$ (2 wt%) and partially for pure $g\text{-C}_3\text{N}_4$ (Fig. S6†). This further supports the presence and importance of chemical bonding between $g\text{-C}_3\text{N}_4$ and Ni_2P .

The SEM image (Fig. 3a) does not show the presence of Ni_2P particles in the $g\text{-C}_3\text{N}_4/\text{Ni}_2\text{P}$ (2 wt%) hybrid due to the low Ni_2P loading content. However, the presence of Ni_2P is clearly demonstrated by energy dispersive X-ray spectroscopy (EDS) as shown in Fig. 3b. A higher Ni_2P content leads to a heavier coverage of the $g\text{-C}_3\text{N}_4$ surfaces (Fig. S7†). Ni_2P loading was further supported by TEM as shown in Fig. 3c. Ni_2P nanoparticles roughly 20 nm in diameter were intimately attached to the $g\text{-C}_3\text{N}_4$ surfaces. It should be noted that the $g\text{-C}_3\text{N}_4/\text{Ni}_2\text{P}$ (2 wt%) sample was ultrasonicated for 40 minutes prior to TEM observation, which supports the strong adhesion of Ni_2P onto $g\text{-C}_3\text{N}_4$. High resolution TEM shows a lattice fringe of 0.507 nm, indexed to the (100) planes Ni_2P (Fig. 3d). EDS shows a Ni/P molar ratio of 1.74 : 1, which is very close to 2 : 1 (Fig. 3b). Elemental mapping further supports the uniform distribution of Ni_2P (see Fig. S8†). The Ni_2P particles grew into large particles

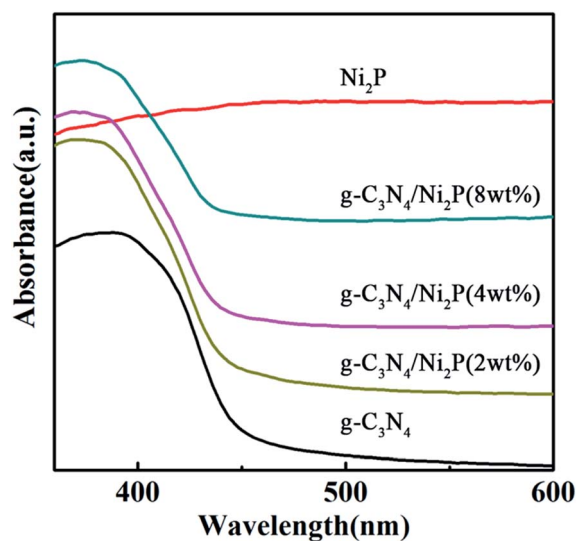


Fig. 2 UV-vis absorption spectra of pure $g\text{-C}_3\text{N}_4$ and $g\text{-C}_3\text{N}_4/\text{Ni}_2\text{P}$ composites with different Ni_2P contents (2 wt%, 4 wt%, and 8 wt%). Pure Ni_2P is included for reference.

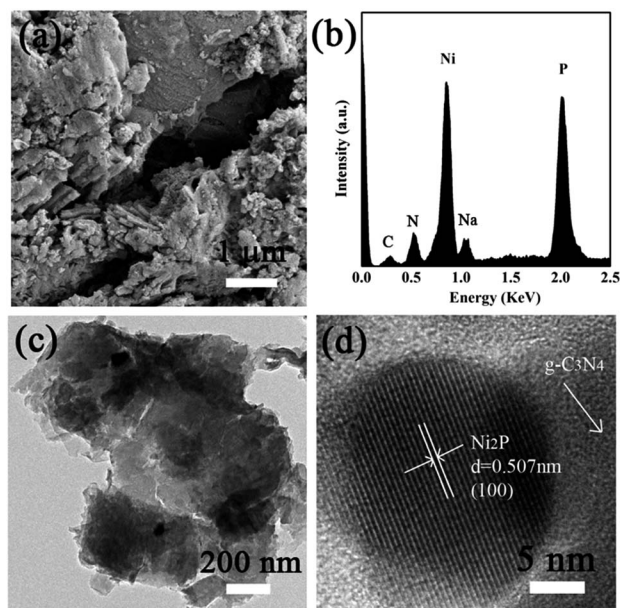


Fig. 3 (a) SEM image of $g\text{-C}_3\text{N}_4/\text{Ni}_2\text{P}$ (2 wt%), (b) EDS spectrum of pure Ni_2P , (c) TEM image of the $g\text{-C}_3\text{N}_4/\text{Ni}_2\text{P}$ (2 wt%) sample, (d) HRTEM image of loaded Ni_2P in the $g\text{-C}_3\text{N}_4/\text{Ni}_2\text{P}$ (2 wt%) sample. The Na signal originates from the incomplete removal of some of the starting material.

and are aggregated at higher degrees of loading, as shown in the $g\text{-C}_3\text{N}_4/\text{Ni}_2\text{P}$ (8 wt%) sample (Fig. S9†).

In order to verify the effect of Ni_2P loading on H_2 evolution, $g\text{-C}_3\text{N}_4/\text{Ni}_2\text{P}$ samples were measured for visible-light-driven ($\lambda > 420$ nm) photocatalytic H_2 generation from water reduction. TEOA (10 vol%) was used as a sacrificial reagent.¹⁵ Control experiments show no H_2 evolution without $g\text{-C}_3\text{N}_4/\text{Ni}_2\text{P}$ catalysts or light irradiation. The photocatalytic H_2 generation rate was controlled by the TEOA concentration (Fig. 4a). The highest H_2 generation rate of $82.5 \mu\text{mol h}^{-1} \text{g}^{-1}$ was achieved when using a $g\text{-C}_3\text{N}_4/\text{Ni}_2\text{P}$ (2 wt%) sample from 10 vol% TEOA solution. All experiments were carried out under these conditions.

Fig. 4b illustrates the average H_2 generation rate of $g\text{-C}_3\text{N}_4/\text{Ni}_2\text{P}$ samples over the first three hours. Pure $g\text{-C}_3\text{N}_4$ samples showed very poor H_2 generation properties (only trace amounts of H_2 were detected). Similarly, Ni_2P alone also has no H_2 generation properties under visible light irradiation. For $g\text{-C}_3\text{N}_4/\text{Pt}$ (0.5 wt%) and $g\text{-C}_3\text{N}_4/\text{Pt}$ (2 wt%), the H_2 generation rates are 72 and $63.5 \mu\text{mol h}^{-1} \text{g}^{-1}$, respectively (Fig. 4b, only the value for the $g\text{-C}_3\text{N}_4/\text{Pt}$ (0.5 wt%) sample is incorporated for conciseness). However, for $g\text{-C}_3\text{N}_4/\text{Ni}_2\text{P}$ (2 wt%), the H_2 evolution rate was enhanced to $82.5 \mu\text{mol h}^{-1} \text{g}^{-1}$, which is superior to that of $g\text{-C}_3\text{N}_4/\text{Pt}$ (0.5 wt%) despite being more naturally abundant and less expensive. It is also essential to emphasize the importance of the *in situ* formation of the Ni_2P particles for the improved performance. In a simple physical mixture of Ni_2P (2 wt%) and $g\text{-C}_3\text{N}_4$, only trace H_2 generation was observed under identical experimental conditions (not shown in Fig. 4b). This underscores the importance of thermal annealing which enables the formation of intimate $\text{Ni}_2\text{P}/g\text{-C}_3\text{N}_4$ interfaces for effective charge transfer from excited $g\text{-C}_3\text{N}_4$ to Ni_2P , which is

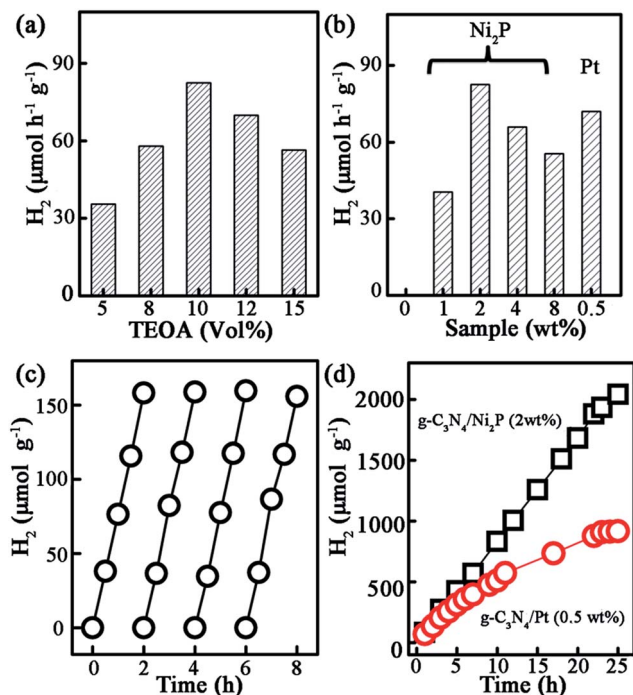


Fig. 4 (a) Photocatalytic H₂ evolution from solutions containing various amounts of TEOA on g-C₃N₄/Ni₂P (2 wt%) under visible light irradiation. (b) Effect of the Ni₂P loading content on photocatalytic H₂ generation from g-C₃N₄. In addition, g-C₃N₄/Pt (0.5 wt%) was also included for reference. The x-axis shows the loading amount of Ni₂P and Pt. (c) Cycling runs for photocatalytic H₂ generation on g-C₃N₄/Ni₂P (2 wt%) under visible light irradiation. (d) Long-term (24 h) H₂ generation on g-C₃N₄/Ni₂P (2 wt%) and g-C₃N₄/Pt (0.5 wt%) under visible light irradiation with a noticeable rate reduction for the latter.

the ultimate cause for enhanced H₂ generation rates. Higher Ni₂P loading on g-C₃N₄ leads to larger interfacial areas, more effective separation of photo-generated electrons and holes and enhanced photocatalytic activity. When the Ni₂P loading content is further increased to 4 wt%, a reduction in hydrogen generation performance is observed. This result is explained by an emergent shielding effect in which overloading by Ni₂P can reduce light absorption of the g-C₃N₄ photocatalyst. In addition, the coverage of the active sites by the Ni₂P co-catalyst also hinders H₂ generation.²⁸

The photo-stability of a co-catalyst is also essential for practical use. Therefore, we examined the stability of Ni₂P as a co-catalyst for photocatalytic H₂ generation with g-C₃N₄/Ni₂P (2 wt%) used as a representative sample. Impressively, g-C₃N₄/Ni₂P (2 wt%) shows highly stable photocatalytic H₂ generation with no decrease in the H₂ generation rate observed over the duration of the experiments (Fig. 4c and d). The cyclic H₂ generation experiments also show consistent and repeatable H₂ generation rates (see Fig. 4c) over four cycles (Fig. 4d). XRD analysis confirmed the unchanged phases of g-C₃N₄/Ni₂P (2 wt%) before and after the 24 h long-term photocatalytic H₂ generation experiments (Fig. S10†). Moreover, no aggregation or morphology changes in Ni₂P occurred during 24 h long-term H₂ generation experiments. This further supports the stability of Ni₂P as a non-noble metal co-catalyst useful in enhancing H₂

generation (Fig. S11†). In comparison, g-C₃N₄/Pt (0.5 wt%) shows a pronounced decrease in the H₂ generation rate throughout the long-term testing (Fig. 4d). TEM shows no aggregation of Pt in g-C₃N₄/Pt (0.5 wt%) after 24 hour H₂ generation experiments (Fig. S12†). This suggests that the Pt co-catalyst present in the system is deactivated during H₂ generation over long-term experiments. These results highlight the excellent stability of Ni₂P as a non-noble metal co-catalyst for enhanced H₂ generation.

Mechanism of enhanced photocatalytic activity

The enhanced photocatalytic H₂ generation is likely a result of the effective interfacial charge transfer from photo-excited g-C₃N₄ to the Ni₂P co-catalyst. It has been reported that the photo-generated electrons can efficiently transfer from the conduction band (CB) of CdS to Ni₂P.²⁹ Since the CB edge of g-C₃N₄ (−1.2 V vs. the NHE) is more negative than that of CdS (−0.5 V vs. the NHE),³⁰ the photo-excited electrons on g-C₃N₄ could thus transfer to Ni₂P through the g-C₃N₄/Ni₂P interfaces created by annealing (Fig. 5). The electrons accumulating on the Ni₂P particles can then reduce H⁺ into hydrogen while the holes on g-C₃N₄ can oxidize the sacrificial electron donor TEOA. The effective separation of the photo-generated electrons and holes in g-C₃N₄ further improves photocatalytic H₂ generation.

Interfacial charge transfer is evident from the decreased photoluminescence (PL) intensity in g-C₃N₄/Ni₂P (2 wt%) (Fig. 6a) as compared to pure g-C₃N₄. Pure g-C₃N₄ emits a strong PL peak at 472 nm. Ni₂P integration can significantly quench this peak (Fig. S13†). In addition, the PL peak shifts from 472 nm for pure g-C₃N₄ to 467 nm for g-C₃N₄/Ni₂P (2 wt%). This peak shift is caused by Ni₂P addition, as evidenced by the PL peak of the g-C₃N₄ and Ni₂P (2 wt%) mixture (Fig. S13†). As expected, Pt loading can also reduce the PL of g-C₃N₄, but the peak position remains unchanged with respect to pure g-C₃N₄ (Fig. S13†). This strong chemical interaction between g-C₃N₄ and Ni₂P affects the Stokes shift of g-C₃N₄ leading to the blue shift in the PL peak. This interaction is currently being evaluated by density functional theory (DFT) calculations. The PL spectra clearly originate from the intimate contact between Ni₂P and g-C₃N₄ which facilitates the photo-induced electron transfer from g-C₃N₄ to Ni₂P.

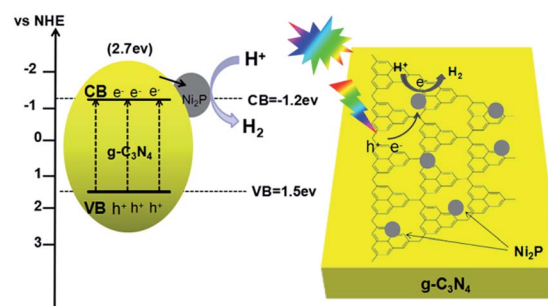


Fig. 5 Schematic illustration of the (left) energy position of g-C₃N₄ vs. the normal hydrogen electrode (NHE) and (right) charge transfer from photo-excited g-C₃N₄ to Ni₂P particles for H₂ evolution.

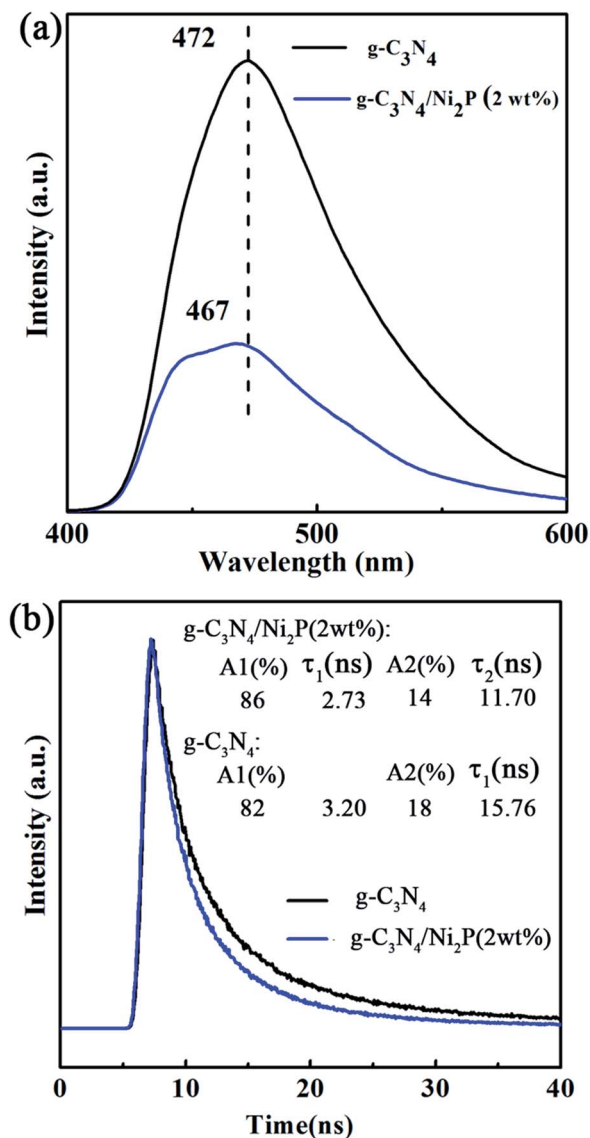


Fig. 6 (a) Stable photoluminescence spectra and (b) time-resolved photoluminescence decay spectra of pure $g\text{-C}_3\text{N}_4$ and $g\text{-C}_3\text{N}_4/\text{Ni}_2\text{P}$ (2 wt%) measured in the solid state. The fitted lifetime from the fluorescence decay is also presented.

The interfacial charge transfer can be further understood by the decreased PL lifetime (Fig. 6b). The average lifetime of pure $g\text{-C}_3\text{N}_4$ and $g\text{-C}_3\text{N}_4/\text{Ni}_2\text{P}$ (2 wt%) are 5.43 and 3.95 ns, respectively. The decreased PL lifetime shows the rapid charge transfer in Ni_2P -loaded $g\text{-C}_3\text{N}_4$,³¹ which reduces the recombination of photo-generated electron-hole pairs. Furthermore, the lifetime of $g\text{-C}_3\text{N}_4/\text{Ni}_2\text{P}$ (2 wt%) is shorter than that of $g\text{-C}_3\text{N}_4/\text{Ni}_2\text{P}$ (8 wt%) (4.08 ns) (Fig. S14[†]). This result is also consistent with the observed photocatalytic H_2 generation plots (Fig. 4b). The PL decay spectra together with the stable PL spectra clearly demonstrate that Ni_2P can serve as an efficient noble-metal free co-catalyst to harvest the electrons from photo-excited $g\text{-C}_3\text{N}_4$ and further catalyze proton reduction into H_2 .

Conclusions

In summary, $g\text{-C}_3\text{N}_4/\text{Ni}_2\text{P}$ hybrids can be facilely prepared via a single-step annealing process. Ni_2P nanoparticles can serve as an active and highly stable non-noble metal co-catalyst for improving H_2 generation on $g\text{-C}_3\text{N}_4$. The enhancement was mainly attributed to efficient charge transfer from photo-excited $g\text{-C}_3\text{N}_4$ to Ni_2P , which suppressed the recombination of electron-hole pairs in $g\text{-C}_3\text{N}_4$. This work shows the great potential of noble-metal free Ni_2P for improving photocatalytic H_2 generation of $g\text{-C}_3\text{N}_4$ and provides new insights into developing low cost and highly efficient transition-metal phosphides as co-catalysts for enhanced photocatalytic water-splitting.

Acknowledgements

This work was financially supported by the National Natural Science Foundation of China (51572003), Anhui Provincial Natural Science Foundation (1508085ME105, 1408085MB22), SRF for ROCS, SEM, and Technology Foundation for Selected Overseas Chinese Scholars, Ministry of Personnel of China. Dr Yuan acknowledges the China Scholarship Council for financial support.

Notes and references

- X. B. Chen, S. H. Shen, L. J. Guo and S. S. Mao, *Chem. Rev.*, 2010, **110**, 6503–6570.
- A. Kudo and Y. Miseki, *Chem. Soc. Rev.*, 2009, **38**, 253–278.
- Y. P. Yuan, L. W. Ruan, J. Barber, S. C. J. Loo and C. Xue, *Energy Environ. Sci.*, 2014, **7**, 3934–3951.
- F. E. Osterloh, *Chem. Soc. Rev.*, 2013, **42**, 2294–2320.
- S. Cao, J. Low, J. Yu and M. Jaroniec, *Adv. Mater.*, 2013, **27**, 2150–2176.
- X. Li, J. G. Yu and M. Jaroniec, *Chem. Soc. Rev.*, 2016, **45**, 2603–2636.
- J. Hu, A. Liu, H. Jin, D. Ma, D. Yin, P. Ling, S. Wang, Z. Lin and J. Wang, *J. Am. Chem. Soc.*, 2015, **137**, 11004–11010.
- M. Ye, J. Gong, Y. Lai, C. Lin and Z. Lin, *J. Am. Chem. Soc.*, 2012, **134**, 15720–15723.
- Y. Guo, J. Li, Y. Yuan, L. Li, M. Zhang, C. Zhou and Z. Lin, *Angew. Chem., Int. Ed.*, 2016, **55**, 14693–14697.
- S. K. Lee and A. Mills, *Platinum Met. Rev.*, 2003, **47**, 61–72.
- J. H. Yang, D. Wang, H. X. Han and C. Li, *Acc. Chem. Res.*, 2013, **46**, 1900–1909.
- J. R. Ran, J. Zhang, J. G. Yu, M. Jaroniec and S. Z. Qiao, *Chem. Soc. Rev.*, 2014, **43**, 7787–7812.
- P. W. Du and R. Eisenberg, *Energy Environ. Sci.*, 2012, **5**, 6012–6021.
- L. S. Yin, Y. P. Yuan, S. W. Cao, Z. Y. Zhang and C. Xue, *RSC Adv.*, 2014, **4**, 6127–6132.
- Y. P. Yuan, S. W. Cao, L. S. Yin, L. Xu and C. Xue, *Int. J. Hydrogen Energy*, 2013, **38**, 7218–7223.
- S. Cao, Y. Chen, C. C. Hou, X. J. Lv and W. F. Fu, *J. Mater. Chem. A*, 2015, **3**, 6096–6101.
- S. Cao, Y. Chen, C. J. Wang, P. He and W. F. Fu, *Chem. Commun.*, 2014, **50**, 10427–10429.

- 18 E. J. Popczun, J. R. McKone, C. G. Read, A. J. Biacchi, A. M. Wiltrout, N. S. Lewis and R. E. Schaak, *J. Am. Chem. Soc.*, 2013, **135**, 9267–9270.
- 19 Y. Liang, Q. Liu, A. M. Asiri, X. Sun and Y. Luo, *ACS Catal.*, 2014, **4**, 4065–4069.
- 20 J. Tian, Q. Liu, A. M. Asiri and X. Sun, *J. Am. Chem. Soc.*, 2014, **136**, 7587–7590.
- 21 J. Tian, Q. Liu, N. Cheng, A. M. Asiri and X. Sun, *Angew. Chem., Int. Ed.*, 2014, **53**, 9577–9581.
- 22 P. Xiao, M. A. Sk, L. T. Thia, X. Ge, R. J. Lim, J. Y. Wang, K. H. Lim and X. Wang, *Energy Environ. Sci.*, 2014, **7**, 2624–2629.
- 23 S. Ye, R. Wang, M. Z. Wu and Y. P. Yuan, *Appl. Surf. Sci.*, 2015, **358**, 15–27.
- 24 Y. Zheng, H. Li, B. Wang and X. C. Wang, *Angew. Chem., Int. Ed.*, 2015, **54**, 12868–12884.
- 25 Y. Sasaki, A. Iwase, H. Kato and A. Kudo, *J. Catal.*, 2008, **259**, 133–137.
- 26 H. Zhao, S. Sun, P. Jiang and Z. J. Xu, *Chem. Eng. J.*, 2017, **315**, 296–303.
- 27 A. L. Han, H. L. Chen, Z. J. Sun, J. Xu and P. W. Du, *Chem. Commun.*, 2015, **51**, 11626–11629.
- 28 X. L. Liu, R. Wang, G. S. Xu, C. H. Li, Y. P. Yuan and C. Xue, *APL Mater.*, 2015, **3**, 114403.
- 29 W. Z. Gao, Y. Xu, Y. Chen and W. F. Fu, *Chem. Commun.*, 2015, **51**, 13217–13220.
- 30 S. W. Cao, Y. P. Yuan, J. Fang, M. M. Shahjamali, F. Y. C. Boey, J. Barber, S. C. J. Loo and C. Xue, *Int. J. Hydrogen Energy*, 2013, **38**, 1258–1266.
- 31 Z. J. Sun, H. F. Zheng, J. S. Li and P. W. Du, *Energy Environ. Sci.*, 2015, **8**, 2668–2676.